Highlight on commercial SERS substrates and on optimized nanorough large-area SERS-based sensors: a Raman study

M. Rahmani, P. Taugeron, A. Rousseau, N. Delorme, L. Douillard, L. Duponchel, J.-F. Bardeau

▶ **To cite this version:**

M. Rahmani, P. Taugeron, A. Rousseau, N. Delorme, L. Douillard, et al.. Highlight on commercial SERS substrates and on optimized nanorough large-area SERS-based sensors: a Raman study. Applied Nanoscience, 2023, n.a, 10.1007/s13204-023-02972-6 . hal-04301407

HAL Id: hal-04301407
https://hal.science/hal-04301407

Submitted on 23 Nov 2023

HAL is a multi-disciplinary open access archive for the deposit and dissemination of scientific research documents, whether they are published or not. The documents may come from teaching and research institutions in France or abroad, or from public or private research centers.

L'archive ouverte pluridisciplinaire **HAL**, est destinée au dépôt et à la diffusion de documents scientifiques de niveau recherche, publiés ou non, émanant des établissements d'enseignement et de recherche français ou étrangers, des laboratoires publics ou privés.

Highlight on commercial SERS substrates and on optimized nanorough large-area SERS-based sensors: A Raman study

M. Rahmani[†], P. Taugeron[†], A. Rousseau[†], N. Delorme[†], L. Douillard[‡], L. Duponchel[††], J.-F. Bardeau[†*]

[†]Institut des Molécules et Matériaux du Mans – CNRS UMR 6283, Univ. Le Mans, F-72085 Le Mans, France

[‡]Université Paris-Saclay, CEA SPEC, CNRS UMR 3680, F-91190 Gif-sur-Yvette, France

[††] Université de Lille, CNRS UMR 8516 – LASIRE – Laboratoire de Spectroscopie pour Les Interactions, La Réactivité et L'Environnement, Lille, F-59000, France.

Corresponding Author

*E-mail: Jean-Francois.Bardeau@univ-lemans.fr

KEYWORDS

SERS, commercial substrates, nanorough surface, trace detection, Raman analysis

ABSTRACT

Surface Enhanced Raman Spectroscopy (SERS) is a powerful non-invasive technique to detect and identify molecule traces. The accurate identification of molecules is based on the detection of distinctive vibrational modes characteristic of a molecule adsorbed onto the surface. We investigated the detection performances of three commercial SERS substrates: nanostructured Au supports from Hamamatsu, Premium Ag-Au supports from SERSitive, and RAM-SERS-Au from Ocean Insight, which were tested with solutions of thiophenol (C_6H_6S) at 10^{-6} M and 10^{-8} M concentration. SERS measurements were performed systematically with 633 and 785 nm excitation wavelengths and Raman mappings were recorded randomly on the surfaces. The

spectral quality (baseline intensity and signal-to-noise ratio), the thermal stability under laser illumination, and the Raman intensity distribution of the Hamamatsu substrate and our own fabricated gold substrate were discussed for the detection of 10^{-8} M thiophenol molecules. The detection of crystal violet (CV), a toxic dye, is demonstrated at 5.10^{-9} M.

INTRODUCTION

Surface Enhanced Raman Spectroscopy (SERS) was discovered in 1974 (Fleischmann et al. 1974). It's a non-destructive, ultra-sensitive, and free-label technique for detecting and identifying materials and analytes (Fleischmann et al. 1974; Albrecht and Creighton 1977; Jeanmaire and Van Duyne 1977). It has been extensively used for the trace-level detection of explosives (Dasary et al. 2009), environmental pollutants (Halvorson and Vikesland 2010; Hou et al. 2015), food safety (Sun et al. 2017; Chen et al. 2019; Lin and He 2019) and much more by developing specific affinities between targets and the surface of SERS substrates (Wang et al. 2020). It still attracts today's research communities (Gillibert et al. 2018; Bodelón and Pastoriza-Santos 2020; Pérez-Jiménez et al. 2020; Mandal and Tewari 2022) for the development of new applications and fundamental aspects. The SERS phenomenon is based on two main mechanisms. First, a chemical effect arises when the polarizability of an analyte molecule is modulated due to a charge transfer mechanism between the substrate and the molecule (Kim et al. 2019). Second, an electromagnetic mechanism, mainly due to the interaction between the incident light and the metallic nanoparticles (NPs) induces the excitation of *localized surface plasmons* (LSP) resulting in amplification of the electric field E in the vicinity of particles surfaces (Sreekanth et al. 2016; Ding et al. 2017). The so-called "hot spots" can be created when the space between two or more NPs is very narrow or on a surface presenting heterogeneities at the nanometric scale (Grésillon et al. 1999). The largest electromagnetic enhancement is obtained when inter-particle gap dimensions are less than 5 nm

and in this case, if a molecule is in the vicinity of the hot spots, strong Raman signal enhancements (from 4 to 11 orders of magnitude) can be observed (Ding et al. 2017).

Several strategies have emerged over the past decade to develop solid SERS substrates. The most cost-effective and simple method is to use solutions of colloidal nanoparticles to fabricate colloidal assemblies on a substrate (Ye et al. 2021). Many efforts have been made to better understand the mechanisms involved in the self-organization of nanoparticles into well-ordered geometries, the most effective approaches for developing real applications with different 2D or 3D patterning (Chen et al. 2018). Unfortunately, it is still relatively difficult to induce and control the quality of nanoparticle arrays, and thus inter-particle gaps at nanoscale, over a large surface area due to inhomogeneities of the distributions in size and shape of the particles. Nevertheless, although the uncontrolled density of hot spots often results in variations in Raman signal intensity, these shortcomings have not prevented this technique from being widely used in applications (He et al. 2015).

Other techniques have been used to create SERS-active substrates, such as electrochemical syntheses that produce different random nanostructured surfaces like ZnO nanorods decorated with Au nanoparticles (Yi et al. 2014) or Ag nanoislands formed on SiO_2 glass (Zhurikhina et al. 2012). Periodic nanostructures with excellent reproducibility and sensitivity have also been developed by using sophisticated and expensive microfabrication techniques like electron beam lithography (Abu Hatab et al. 2008; Wu and Lin 2018), ion beam lithography (Sivashanmugan et al. 2013), and laser ablation (Byram et al. 2017). Although the sensitivity of these SERS-active substrates is widely recognized, most of the SERS applications are still severely limited by the low reproducibility, very small active area and high manufacturing cost of substrates.

Today, numerous commercial SERS substrates can be purchased. Substrate manufacturing processes are generally different, the surface quality not equivalent, nor are the enhancement factors and the reproducibility from one batch to another. A few works reported on the

reproducibility of the Raman signal recorded on commercial substrates after immersion in 10^{-4} M sample solutions (Liu et al. 2020) and more recently on the sensing performances of commercial SERS substrates (Liszewska et al. 2019; Azziz et al. 2022) some of which having *limits of detection* (LOD) in the range of 10^{-5} - 10^{-6} M. We believe it is important to continue these investigation works to provide new users with relevant information to select suitable SERS media, when the molecular concentration is typically in the 10^{-6} - 10^{-8} M range. In addition, we would like to demonstrate that it is possible to prepare in laboratory, with a minimum set-up, substrates allowing the detection of molecules from solutions at 10^{-8} - 10^{-9} M. The interest is all the more important today as the detection and identification of pollutant residues in this concentration range has become a necessity if we refer to the limits established by the Directive 2000/60/EC of the European Parliament (2000).

The fabrication of efficient and reproducible SERS substrates with a large surface area, that can be used over a wide concentration range, is not an easy task. Quantitative sensing analyses require high reproducibility in 2D-3D topographic features to generate similar hot spot surface densities and intensity distribution from sample to sample under the same experimental conditions. Photoemission electron microscopy (PEEM), a high-resolution near-field mapping technique (Douillard et al. 2007; Awada et al. 2012), can be used to collect high-contrast electronic images reflecting the distribution of hot spots on a sample surface at a subwavelength scale. Recently, this technique was used for studying the variation in hot spot density per unit area of an Au film as a function of the process conditions (Taugeron et al. 2023). We were able to optimize nanorough Au film substrates fabricated by *physical vapor deposition* (PVD) and show, for the first time of our knowledge, that the near field optical responses of our bare fresh surfaces are quantitatively correlated with their far field Raman diffusion signature when they are used as molecular sensors.

In the present paper, we investigate the detection efficiency of three different commercial SERS substrates: Hamamatsu, Premium Ag-Au from SERSitive, and RAM SERS Au from Ocean Insight. As a standard target molecule, thiophenol in alcoholic solution diluted at 10^{-6} M and 10^{-8} M is used. This molecule is commonly used for SERS analysis because it adsorbs easily on the gold surface via its thiol function to form, on a flat surface when the concentration is high enough, an homogeneous layer after rinsing (Noh et al. 2010; Taugeron et al. 2023). For 10^{-8} M thiophenol solutions, we will be in more drastic detection conditions since it will be impossible to cover the entire active surface of our substrates with a homogeneous and dense layer of molecules. These will therefore be perfect conditions to objectively and quantitatively compare the performance of our optimized home-made nanorough substrate to the best commercial substrate. We then discuss the results in terms of spectral quality, signal homogeneity, distribution of intensity and thermal stability under laser beam. Finally, we study the possible detection of traces of crystal violet (CV), in alcoholic solution, a chemical dye and an anti-fungal (exhibiting electronic resonance in the visible region) identified as a biohazardous and a strong carcinogen material (Mani and Bharagava 2016).

MATERIALS AND METHODS

Commercial SERS substrates

Nanoimprinted substrates were purchased from Hamamatsu Photonics (Japan); each substrate was vacuum sealed. Premium-Ag-Au substrates purchased from SERSitive (Poland) are stored in Air conditions, packed into small microcentrifuge tubes and stored in vacuum package. RAM SERS-Au substrates were purchased from Ocean Insight (USA), wrapped and vacuum sealed (Fig S1).

Nanorough Au substrate fabrication

Our home-made substrates are fabricated by physical vapor deposition (thermal evaporation) of Au. The fabrication method was recently reported (Taugeron et al. 2023). Briefly, the samples are prepared by a reproducible two-step thermal evaporation process: A Au layer of approximately 100 nm is first deposited on a Si wafer (the film thickness being controlled by a quartz microbalance system) with a rate of 0.1 nm/s at a pressure of 5.10^{-6} mbar. The Au/Si reference substrate is then cut into small pieces of about 8 x 8 mm^2. On each piece, an additional Au deposition of 8-9 nm (close to the film percolation threshold) is carried out.

Surface functionalization

Thiophenol (97%, ACROS), resp. crystal violet (CV) (ACS reagent, ≥ 90% anhydrous basis, Sigma-Aldrich), are diluted with ethanol (99.8%, Sigma-Aldrich) to prepare respectively a 10^{-3} M thiophenol and a 10^{-3} M CV solutions. The diluted solutions from 10^{-5} to 10^{-9} M are prepared by serial dilution. To avoid any surface contamination, our homemade substrates are used after Au deposition and the commercial SERS substrates just after being opened from their packaging. For each concentration, the substrates are immersed in 2 ml of the prepared solutions for 10 minutes, then rinsed into both ethanol (30 s) and ultrapure water (30 s) (to remove non-

specific binding molecules) and then dried at room temperature. The functionalized substrates are then studied by Raman imaging without any additional cleaning.

Raman analysis

Raman measurements are performed using a confocal Raman spectrometer Witec alpha 300R with excitation wavelengths at 632.8 (He-Ne laser) and 785 nm (laser diode). The Raman spectra are recorded in the air using 1) a x50 long Working Distance (W.D. = 9 mm) magnification objective (N.A. = 0.55) to compare the commercial substrates with each other and 2) a Zeiss x100 magnification objective (N.A. = 0.9, W.D. = 0.28 mm) to compare the efficiency of Hamamatsu and our nanorough substrates to detect molecules from 10^{-8} M solution. The laser power and the acquisition time are adjusted from one substrate to another (Table S1 and S2) to avoid damaging the active SERS surfaces and achieve high signal-to-noise ratio or complete loss of Raman signal. Three different area mappings (20 x 20 µm² with an X and Y step of 1 µm) are systematically acquired on two supports from each SERS substrate. Data processing was done using the Witec Project Five software (version 5.1) including the cosmic ray removal correction function and a shape function for the background subtraction.

Scanning Electron Microscopy

The *scanning electron microscopy* (SEM) images are obtained using a JSM-6510LV microscope (JEOL, Tokyo, Japan). The samples are observed under an accelerating voltage of 20 kV. SEM images are acquired in secondary electron imaging (SEI) at different magnification of 10000X, 15000X or 20000X.

Optical profilometry

The 3D surface scans of the SERSitive and Ocean Insight substrates were undertaken using the confocal white light profilometer S-NEOX (Sensofar-Tech S. L., Barcelona, Spain). The

120×90 μm^2 area were collected using a 150X EPI Nikon objective (N.A. = 0.95). The data were analyzed by the open-source Gwyddion software (version 2.62).

Atomic Force Microscopy

AFM pictures of Hamamatsu and our homemade nanorough substrates were performed by tapping mode in air using a Keysight 5500 AFM (USA). A SuperSharp Silicon Nanosensors™ tip, with a tip curvature radius of 2 nm, was used to record the 3D high-resolution topography of the surface. Image processing was performed using the open-source Gwyddion software (version 2.62).

RESULTS AND DISCUSSION

Comparison of commercial SERS substrates

The three commercial SERS substrates (Hamamatsu, Premium Ag-Au from SERSitive, and RAM SERS Au from Ocean Insight) are fabricated with different techniques. In the following paragraph, their mesoscopic surface topographies are characterized by SEM (Fig.1) and optical profilometry (Fig. S2).

The Hamamatsu® substrate is characterized by a regular array of gold nanostructures, as shown by the SEM imaging (Fig. 1a), consisting of submicrometric nanospheres deposited on a gold substrate. The SERSitive® substrate is made with a mixture of silver and gold nanoparticles deposited randomly and non-uniformly on an indium tin oxide (ITO) glass surface (Fig. 1b). For the Ocean Insight® substrate, we observe polymer fibers covered inhomogeneously with gold nanoparticles (Fig. 1c). From the optical profilometry images (Fig. S2), it is easy to

visualize the open 3D architecture for the SERSitive® and Ocean Insight® substrates; the maximum heights are about 2.7 ± 0.3 µm and 22± 5 µm, respectively.

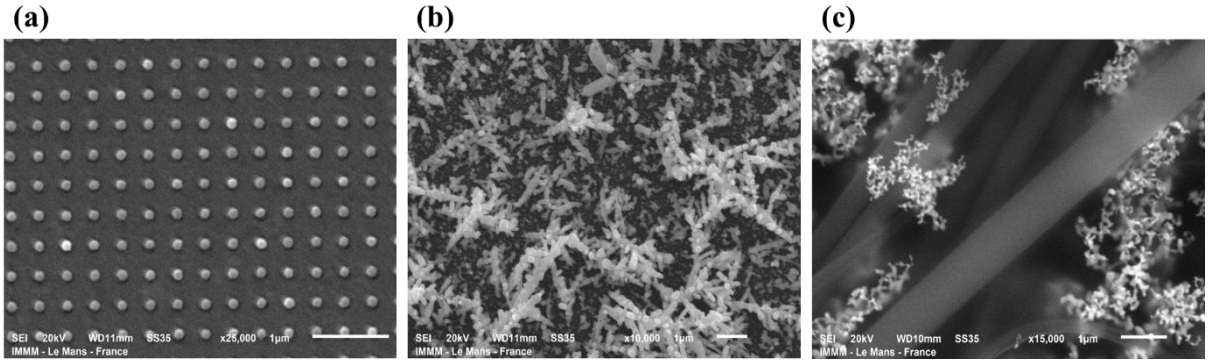

Fig. 1: SEM images of the commercial substrates. (a) Hamamatsu, (b) SERSitive and (c) Ocean Insight. White scale is 1 µm.

To sum up, SERSitive and Ocean Insight substrates exhibit pronounced 3D structures with inhomogeneous surface metal distributions. In contrast, the Hamamatsu substrate has a precise 2D periodic metal architecture with well-controlled nanostructured features. The performance of a SERS substrate depends on a wide range of physical parameters: light wavelength, light irradiance, integration time, response stability, response homogeneity... Therefore, choosing the most efficient substrate for any analytical application remains a challenge. So, in the following experiments, we will attempt to address some of these issues.

We start comparing the Raman signal of the three commercial SERS substrates at 633 nm and 785 nm excitation wavelengths after 10 min immersion in a 10^{-6} M thiophenol solution. The laser power and acquisition time are adjusted for each substrate to avoid surface sample damage and to maximise the signal to noise ratio. Table S1 shows the experimental conditions for each substrate. After depositing the analyte probe molecules, 400 spectra were recorded from a 20 x 20 µm² area mapping with a 2D map step size of 1 µm. For each substrate, three maps are recorded on different areas. In order to compare the performance of the commercial substrates, the average Raman spectra shown in Fig. 2 are normalized i.e. each recorded spectrum was

divided by the laser power value and the acquisition time. The average spectra with the baseline are reported in Fig. S3a. The distinctive Raman bands corresponding to the vibrational modes of thiophenol molecules (Carron and Hurley 1991; Li et al. 2007) can be clearly observed. As already mentioned in literature (Carron and Hurley 1991; Li et al. 2007) the peak at 415 cm^{-1} is attributed to the C-S stretching vibration mode, the peak at 1000 cm^{-1} to the C–H out-of plane bending and ring out-of-plane deformation, the peak at 1025 cm^{-1} to the ring in-plane deformation and C–C symmetric stretching, and the peak at 1075 cm^{-1} to the C–C symmetric stretching and C–S stretching. The peak at 1575 cm^{-1} corresponds to the C=C symmetric stretching mode.

Since the main characteristic peaks of thiophenol are detected at 10^{-6} M for all the substrates, we then compared the relative integrated Raman intensity in the spectral range 350-1800 cm^{-1} (Fig. 3). The highest values are obtained at 633 nm with the Premium Ag-Au from SERSitive and at 785 nm with RAM SERS Au substrate from Ocean Insight. Such results are not surprising, as compared to Hamamatsu substrates their 3D structures and micrometric heights offer a larger specific Au surface on which the analyte molecules can be adsorbed (see SEM and profilometry imagings).

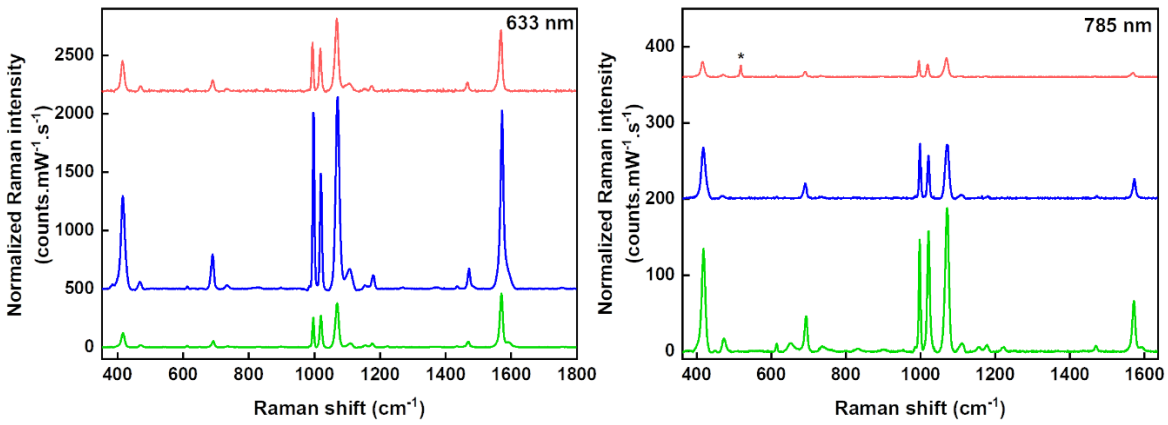

Fig. 2: Average SERS spectra of thiophenol at 10^{-6} M on Hamamatsu (red), SERSitive (blue), and Ocean Insight (green) at two excitation wavelengths: 633 nm (left) and 785 nm (right). The

spectra are vertically shifted for clarity. *The band at 520 cm^{-1} belongs to the Si line below the active gold surface. Spectral intensity is reported in counts (counts) per milliwatt (mW) per second (s) (counts.$mW^{-1}s^{-1}$).

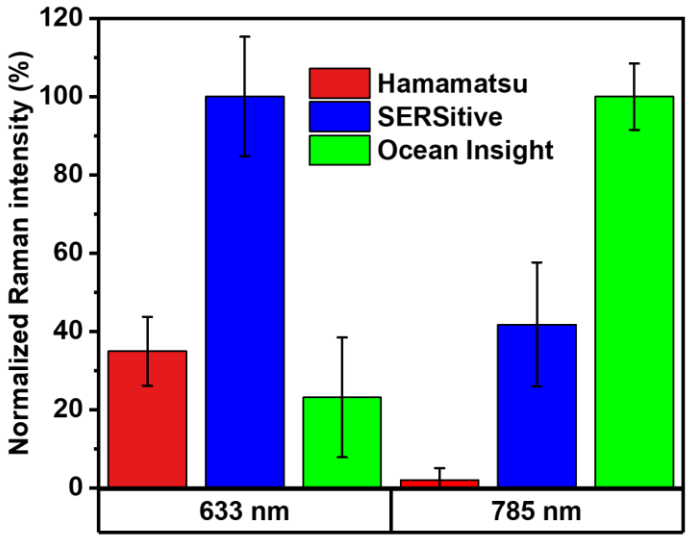

Fig. 3: Comparison of integrated Raman intensity, calculated from Fig.2 in the 350-1800 cm^{-1} spectral range, for the three commercial SERS substrates: Hamamatsu (red), SERSitive (blue), and Ocean Insight (green). The intensity values are independently normalized to each incident wavelength. The Si 520 cm^{-1} line is discarded in the analysis.

Detecting analytes at very low concentrations and recording reliable and reproducible SERS spectra are of great interest for many applications (Rubira et al. 2014; Moram et al. 2020; Kumar and Soni 2022). It is therefore useful to study with precision the ability of these commercial substrates to detect the model molecule at concentrations below 10^{-6} M. In the following, we thus compare their efficiency to detect thiophenol molecules from a 10^{-8} M solution. Table S2 shows the experimental conditions used for each substrate, the acquisition procedure being the same as above. The bare average spectra (without normalization and baseline substraction) are

shown in Fig. S3b and the normalized average Raman spectra are shown in Fig. 4. On the Ocean Insight substrate (green spectra in Fig. 4) it is really difficult to identify (for both 633 and 785 nm excitation wavelengths) the characteristic Raman signature of the thiophenol molecules. At 633 nm, the Hamamatsu substrate is definitely the best substrate to use since it allows to record without any ambiguity and with a relatively good signal-to-noise ratio all the vibrational bands of the target molecules. Let us also noticed that no additional Raman band appears on the spectrum, spurious peak which might interfere with the main vibrational bands of the molecule to detect. At 785 nm, with this substrate, we can nevertheless observe a well-defined band at 520 cm^{-1} assigned to a phonon band of Si (Uchinokura et al. 1972) below the active Au coating.

Despite the low intensities or complex spectra recorded with Ocean Insight and SERSitive, it is nevertheless useful to compare the efficiency of the three commercial substrates. Being not able to do so over the previous spectral range (350-1800 cm^{-1}), we selected the band at 1075 cm^{-1}, since it appears on all three spectra whatever the wavelength used (Fig. 5). The best Raman sensitivity is in favor of the Hamamatsu substrate and this for the two wavelengths, even if the signal is much lower at 785 nm. Such results confirm the recent reported investigations (Liu et al. 2020; Azziz et al. 2022), but here with a lower limit detection: 10^{-8} M.

Regarding SERSitive and Ocean Insight substrates, the detection and especially the identification of the target molecule based on the raw Raman spectrum is more critical at the trace level due to relatively intense spurious bands present on the background spectra. Indeed, the spectrum measured for example on Ocean insight at 785 nm presents a lot of additional bands, similar (but not exactly identical) to what can be observed on the bare surface background spectrum presented in Fig. S4. The disadvantage of these substrates with 3D architecture is therefore that air molecules or particles suspended in the air or in the solvent can unfortunately be more easily captured in the thickness of the layer before or even during Raman analysis and thus cause enhanced Raman scattering that juxtaposes with the characteristic

vibrational modes of target molecules at trace level. Thus, for this reason and under these unconstrained experimental analysis conditions, these two substrates are not suitable for trace detection.

In conclusion, these commercial SERS substrates, with different surface morphologies, can enhance the Raman signal by different orders of magnitude depending on both the concentration of the solutions and the SERS-active surface in contact with the analytes. The choice of a suitable substrate is therefore an important factor to consider before starting the measurements and it appears that SERS substrates based on supported metallic nano-arrays with long-range ordered structures are not always the ones on which the highest Raman intensity will be recorded. Our results confirm, however, that at 10^{-8} M and 633 nm wavelength, the Hamamatsu substrate is the most efficient substrate.

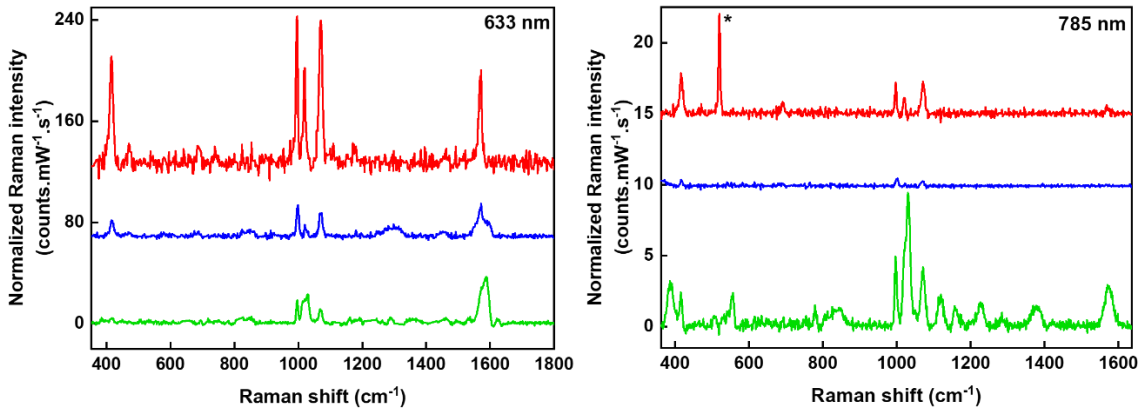

Fig. 4: Average SERS spectra of thiophenol at 10^{-8} M on Hamamatsu (red), SERSitive (blue), and Ocean Insight (green) at two excitation wavelengths: 633 nm (left) and 785 nm (right). The spectra are vertically shifted for clarity. *The band at 520 cm^{-1} belongs to the Si line below the active Au surface. Spectral intensity is reported in counts (counts) per milliwatt (mW) per second (s) (counts.$mW^{-1}s^{-1}$).

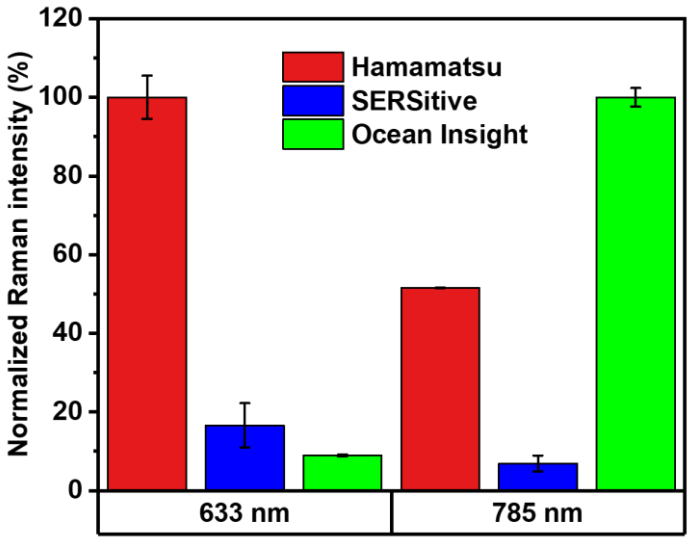

Fig. 5: Comparison of integrated Raman intensity of the vibrational band at 1075 cm^{-1}, for the three commercial SERS substrates: Hamamatsu (red), SERSitive (blue), and Ocean Insight (green). The intensity values are normalized by (i) the laser powers at the incident wavelengths at 633 nm and 785 nm and (ii) the acquisition time.

Performance of our homemade nanorough Au SERS-active substrates

As previously mentioned, we recently reported (Taugeron et al. 2023) on the optimization of nanorough metallic SERS-active substrates fabricated by physical vapor deposition. In the following, the SERS performance of these random metal surfaces is evaluated on the basis of the experimental procedure adopted above for commercial substrates. We verify the efficiency of our nanorough Au substrate using different concentrations of thiophenol from 10^{-5} M to 10^{-9} M. The averaged spectra calculated from the Raman maps and recorded at each concentration are shown in Fig. 6a after baseline substraction. The main thiophenol bands are clearly observed from 10^{-5} M to 10^{-8} M. At 10^{-9} M there are some additional bands in the 1100 – 1700 cm^{-1} region, probably due to surface contamination, as at this level of concentration the surface is not

completely covered with the molecule to be detected. Accordingly, the limit of detection is around 10^{-9} M. The clear identification of the molecule, if based on examination of a raw Raman spectrum with the presence of well-defined vibrational modes, is effective between 10^{-8} M and 10^{-9} M. A linear-log plot of the integrated Raman intensity in the spectral range 1050-1090 cm^{-1} (peak at 1075 cm^{-1}) as a function of thiophenol concentration is shown in Fig. 6b. This result is in agreement with both the results reported by Fedotova et al. using silver nanostructures (Fedotova et al. 2019), Magno et al. using Au/Si nanosensors (Magno et al. 2017), and Barbillon et al. with Au/Si asymmetric dimer array (Barbillon et al. 2021). A decrease in the SERS signal is also observed at 10^{-5} M. This result is consistent with the results of Fedotova et al. after the Au surface (and active hotspots) is covered by a monolayer of molecules; the additional molecules on the surface not being directly in the junctions between the grains (location of hot spots) would then not benefit from the same exaltation factors coming from the surface (Noh et al. 2010; Fedotova et al. 2019).

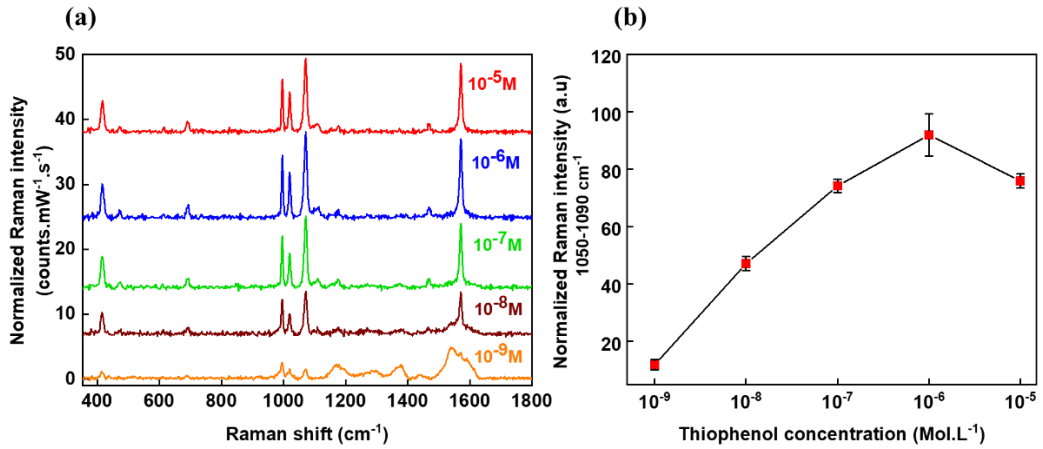

Fig. 6: Our homemade nanorough Au substrate. a) Average SERS spectra of thiophenol at concentrations from 10^{-5} M to 10^{-9} M at 633 nm. The spectra are vertically shifted for clarity. b) Linear-log plot of the integrated Raman intensity in the spectral range 1050 -1090 cm^{-1} as a function of thiophenol concentration. Experimental conditions : 633 nm excitation wavelength, 2 mW laser power, 20 x 20 μm^2 maps, 0.2 s acquisition time.

Spectral analysis on well-controlled and random nanostructured substrates

The two effective substrates for detecting and identifying model molecules at 10^{-8} M are therefore the Hamamatsu substrate and our homemade nanorough Au substrate. The Hamamatsu® substrate is a periodic array of gold nanospheres. The AFM analysis (Fig. 7a) shows that the nanospheres are 225 nm high, deposited on a gold substrate with a period of 500 nm along two axes perpendicular to each other. The surface of our nanorough Au substrate (Fig. 7b) is composed of rounded gold grains (average diameter = 30 nm), exhibits an average surface roughness of 2.0±0.2 nm (Fig. 7).

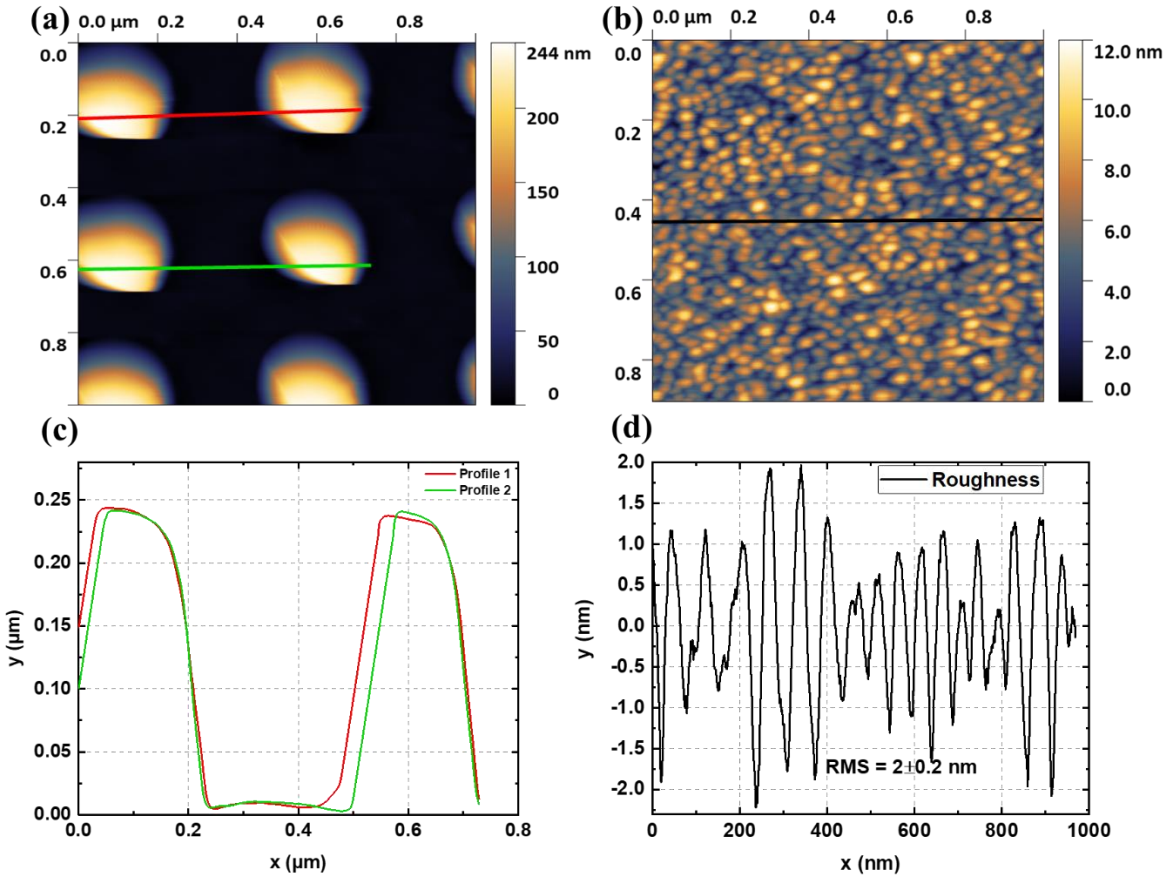

Fig. 7: AFM images of (a) Hamamatsu substrate (1x1 µm-512 points) and (b) our homemade nanorough gold substrate (1x1µm-512 points). Note that, the AFM image of the Hamamatsu

substrate is corrupted in one direction by the geometry of the tip. (c) Height profiles of Hamamatsu substrate and (d) Roughness profile of our homemade nanorough gold substrate.

As previously mentioned, to compare their sensitivity, it is useful to present the average Raman spectra recorded on the two substrates in counts (counts) per milliwatt (mW) per second (s). The normalized spectra shown in Fig. S5 demonstrate that the Hamamatsu SERS substrate is about 8.5 times more efficient than our homemade nanorough gold substrate. However, for the detection (and therefore identification) of trace molecules, beyond the sensitivity of the substrate, the issues of spectral quality and signal stability under irradiation are of major interest. In order to study the stability of the collected Raman signal under irradiation of Hamamatsu and the nanorough Au substrate, we collected Raman signal from a 20 x 20 μm^2 area mapping (400 spectra, with a 2D map step size of 1 μm) after 10 min immersion in a 10^{-8} M thiophenol solution. The experiment is then repeated several times on the same area under the same experimental conditions. For each laser power value, the investigated area was changed.

First, on our homemade nanorough Au substrate, the integration time was fixed to 0.5 s and we acquired systematically 5 maps for 1, 3, 5 and 7 mW laser light incident power. The averaged Raman spectra are reported in Fig. 8a for each laser power. Up to 5 mW and after 5 repetitions no modification of the Raman spectrum (whether in the intensity of the baseline or the vibrational bands) is noted. At 7 mW, the spectral band at 1575 cm^{-1} begins to widen and the intensity of the main vibrational bands decreases with the number of repetitions. The Raman intensity, calculated in the spectral range 977-1097 cm^{-1} to include the bands at 1000, 1025, and 1075 cm^{-1}, is then reported in Fig. 8b. The plot shows a linear relationship between Raman intensity versus laser power, demonstrating that our homemade nanorough substrate is stable under laser irradiation at least up to a laser power of 5 mW (i.e. irradiance of about 2 GW/cm^3 for an estimated analyzed volume of 1 μm^3).

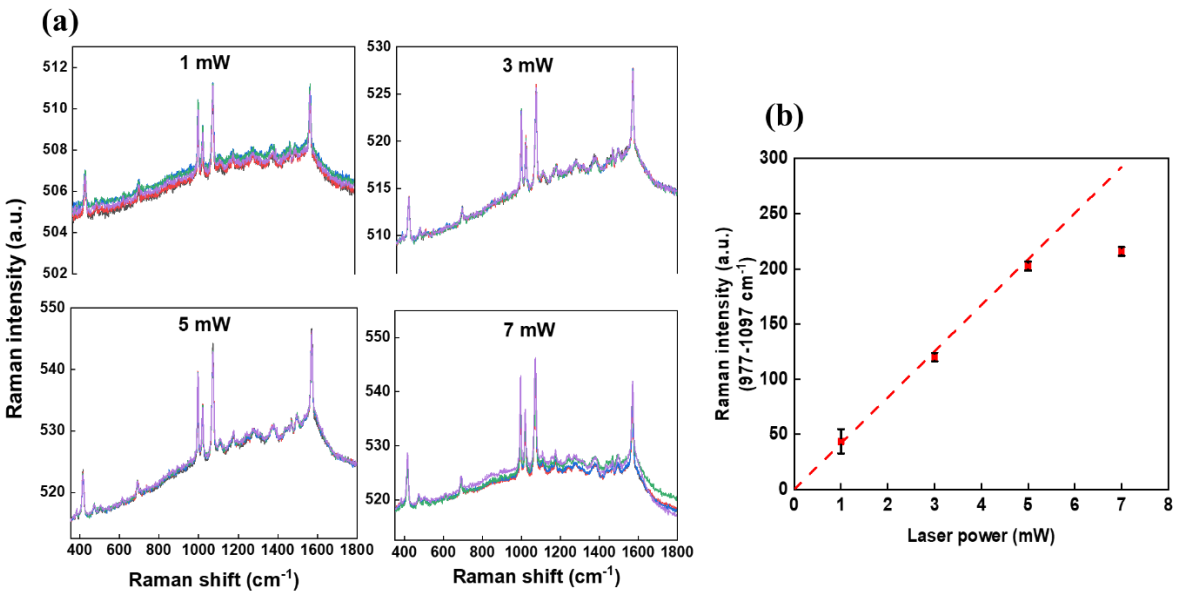

Fig. 8: Our homemade nanorough Au substrate a) Averaged Raman spectra (5 x 20^2 spectra) of thiophenol at 10^{-8} M at 633 nm on the nanorough Au substrate for different laser powers: 1, 3, 5 and 7 mW; b) Plot of the integrated Raman intensity (spectral range 977-1097 cm^{-1}) as function of the laser power fitted with a linear curve (red dashed line).

To check the stability of Hamamatsu SERS substrates under laser beam, we acquire sets of 5 maps (20 µm², 400 spectra, integration time 0.5s) with increasing laser powers 0.03, 0.05, 0.1, 0.15 and 0.2 mW. As before, the location is changed for each laser power. At 0.2 mW laser power, the Raman signal decreases by 50% after the second measurement and the baseline intensity increases (Fig. 9a). Moreover, an optical contrast appears on the substrate (Fig. S6) demonstrating that the Hamamatsu substrate is damaged at such a laser power. This result is not so surprising because in micro-Raman experiments, where the laser light is focused on the micrometer-size area with a high magnification objective, the laser power density can be very high. In our case, where laser output power is about 2 mW, the laser power density can be estimated at sample (in a volume the close to 1 μm^3) to be approximately of the order of 1 GW/cm^3. We previously demonstrated that the structural modifications observed for nanoparticles under high laser irradiation and heat treatment are identical (El Mendili 2011; El

Mendili 2012). Thus, in our case, and in particular for high sensitivity SERS substrates, it is expected that the local temperature of the sample heated under laser excitation (at the laser spot) leads both to surface modifications at the nanoscale and a loss of Raman enhancement. The same surface modification appears on the field of view after the 5^{th} repeated maps for a 0.15 mW power. For 0.03, 0.05 and 0.1 mW power, no damage is visible on the surface after 5 repeated acquisitions and no evident modification of the Raman spectrum is noted (Fig. 9a). The evolution of the integrated Raman intensity over the spectral range 977-1097 cm^{-1} shows a linear scaling with the incident light power (Fig. 9b) from 0.03 mW to 0.1 mW. It then decreases for 0.2 mW due to surface modifications/damages. In short, linear scaling and simple proportional analytical response are only maintain at low light power excitation (up to 0.1 mW).

If by mistake or ignorance the user decides to carry out an experiment with too intense a laser power, he will be confronted with a possible modification of the surface, a loss of the Raman signal and therefore an error in the estimation of the concentration of molecules at the surface and initially in the solution.

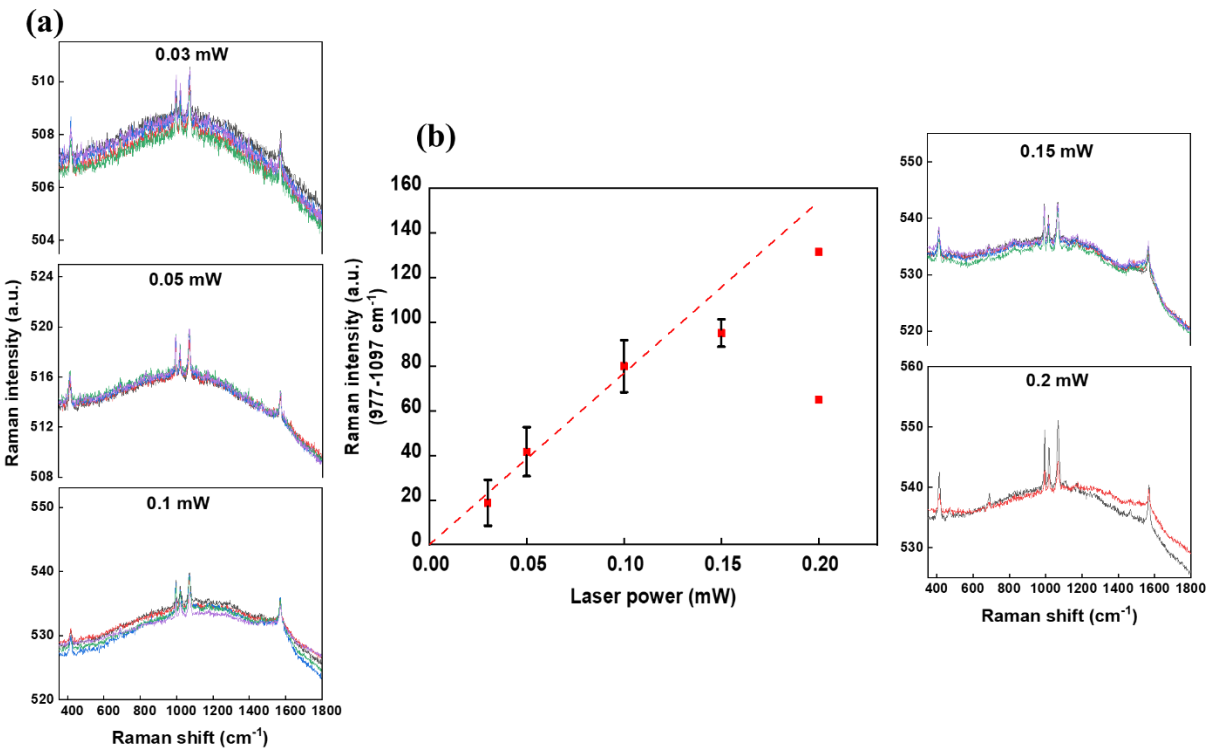

Fig. 9: Hamamatsu SERS substrate. a) Averaged Raman spectra (5 x 20 spectra of thiophenol at 10^{-8} M at 633 nm for 0.03, 0.05, 0.1 and 0.15 mW and only 2 spectra for 0.2 mW due to degradation of the surface after the second map (red) b) Plot of the integrated Raman intensity (spectral range 977-1097 cm^{-1}) as function of the laser power.

Raman intensity distribution analysis

For most applications using SERS technique, researchers mainly rely on the analysis of high quality spectra to get access to structural information and local interactions to monitor physical or chemical reactions (Scherrer et al. 2021; Murugan et al. 2021) or to detect and identify, without ambiguity, traces of analytes. For this type of application, the time allocated to collect the data is often constrained that's why it is important, prior to the setting of the experimental acquisition parameters, to choose the specific SERS-active substrate allowing data to be recorded with the best signal quality. To highlight the importance of this parameter, let us

compare the spectral quality of the data collected under the same experimental conditions (objective X100, 400 spectra recorded in less than 4 min) on the Hamamatsu and our homemade nanorough substrates with the maximum laser powers supported by these substrates, i.e. 0.1 mW and 5 mW respectively. Figure 10a shows the averaged spectra and Figure 10b the Raman intensity distribution of the 400 pixels (20x20 pixels²) map for each substrate. Comparing the SERS intensity histograms, the commercial substrate has a lower collected intensity and a wider distribution, resulting in an overall lower signal-to-noise ratio and lower surface homogeneity than our homemade random metal substrate. In the end, the vibrational modes of the thiophenol molecule are better defined on the nanorough Au substrate.

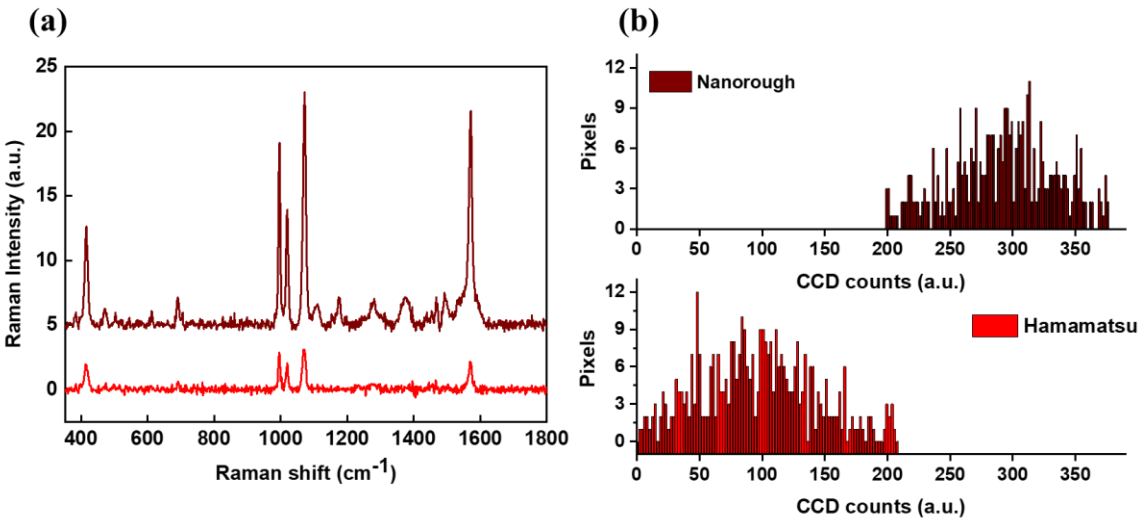

Fig. 10: SERS substrate performances. a) Average SERS spectra of thiophenol at 10^{-8} M on Hamamatsu (red) and our homemade nanorough Au substrate (brown) recorded at 633 nm. The spectra are vertically shifted for clarity. b) Raman intensity histogram distribution for Hamamatsu (red) and our nanorough substrate (brown).

Detection of a toxic dye

To further validate the efficiency of our nanorough Au substrate, we tried to detect crystal violet (CV, $C_{25}H_{30}ClN_3$) molecules at very low concentrations. After 10 min of immersion of the substrates in the CV solutions, we collected Raman spectra on three different areas of the substrates. The average spectrum is plotted against concentration in Fig. 11a after baseline substraction. The characteristic bands of crystal violet appear on all the spectra (Volný et al. 2007; Cañamares et al. 2008) : the band at 421 cm^{-1} is attributed to the out-of-plane bending mode of C-C_{center}-C, the band at 522 cm^{-1} to the bending mode of C-N-C, the band at 914 cm^{-1} to the C-H out-of-plane bending mode and the band at 1367 cm^{-1} to the stretching vibration of nitrogen and phenyl ring. Finally the bands at 1580 and 1615 cm^{-1} are attributed to the in-plane aromatic C-C modes (Volný et al. 2007; Cañamares et al. 2008). In Fig. 11b, we present a log-log plot of the evolution of the Raman intensity as function of the crystal violet concentration. The Raman response increases as a power function of the molar concentration from 5.10^{-9} M to 10^{-6}M.

Since we were able to clearly detect the main vibrational modes of CV at 5.10^{-9} M (Fig. S7), we proved that our homemade substrate is suitable for molecular detection at trace level.

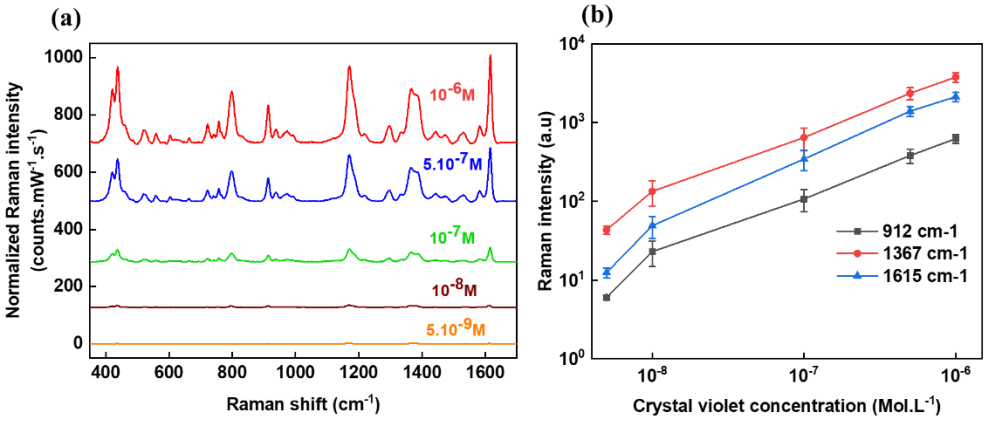

Fig. 11: SERS CV detection substrate performance. a) Average SERS spectra of crystal violet at concentrations from 10^{-6} M and 5.10^{-9} M on the nanorough gold substrate at 633 nm. The spectra are vertically shifted for clarity. b) A log-log plot of the integrated Raman intensity as

a function of CV concentration, for the bands 912 cm^{-1} (black), 1367 cm^{-1} (red) and 1615 cm^{-1} (blue). Experimental conditions: 15 x 15 μm^2 maps, step size 1 µm, 15^2 = 225 spectra per map, laser power 3.9 mW, excitation wavelength 633 nm, acquisition time 0.2 s.

CONCLUSION

To summarize, we investigated the sensing capabilities of three commercial SERS substrates: Hamamatsu from Hamamatsu Photonics, Premium Ag-Au from SERSitive, and RAM-SERS-AU from Ocean Insight, to detect thiophenol as a probe molecule at 10^{-6} M and 10^{-8} M concentration. At the 633 nm and 785 nm excitation wavelengths and 10^{-6} M concentration level, the substrates from SERSitive and Ocean Insight perform better than the Hamamatsu substrate. However, at lower concentrations, their background spectra contain spurious peaks, making trace detection difficult. At 10^{-8} M and 633 nm wavelength, the Hamamatsu substrate is the most efficient (i.e. has the highest enhancement factor) among the investigated substrates. In addition, the figure of merit of a random metal film is evaluated against the Hamamatsu SERS substrate for molecular trace detection. Our optimized homemade nanorough Au film, elaborated by thermal evaporation, has better spectral quality and surface homogeneity and withstands higher laser irradiation. The nanorough Au substrate demonstrates the detection of CV at a 5.10^{-9} M concentration, which ensures that the optimization of this type of substrate, makes it possible to envisage applications in the domains of the environment, health or food safety. Finally, we would like to emphasize that before using Raman intensity to determine the initial concentration of an analyte, it is necessary to determine the laser power range over which there is a linear intensity response and to verify the reproducibility of the measurements at the same location.

Corresponding Author

*E-mail: Jean-Francois.Bardeau@univ-lemans.fr

Author Contributions

Meryem Rahmani: Methodology, Substrates elaborations, Formal analysis, Raman and AFM Investigations, Writing – original draft, Writing – review & editing. **Pierre Taugeron**: Substrates elaborations, AFM investigations, Formal analysis. **Nicolas Delorme**: Methodology, Formal analysis, AFM Investigations, Writing – original draft. **Ludovic Duponchel**: Formal analysis, Writing – original draft. **Ludovic Douillard**: Formal analysis, Writing – original draft. **Jean-François Bardeau**: Conceptualization, Methodology, Raman Investigations, Formal analysis, Writing – original draft, Writing – review & editing, Funding acquisition, Supervision.

Funding Sources

We thank both the AGENCE NATIONALE DE LA RECHERCHE and l'AGENCE FRANCAISE POUR LA BIODIVERSITE (AFB) for having sponsored this study in the frame of the HYDRAE project - ANR – AAP 2019 - CE34 [Grant Number: 192393] and the DIPP-SUF project - [AFB - Grant Number: 197176].

REFERENCES

Abu Hatab NA, Oran JM, Sepaniak MJ (2008) Surface-Enhanced Raman Spectroscopy Substrates Created via Electron Beam Lithography and Nanotransfer Printing. ACS Nano 2:377–385. https://doi.org/10.1021/nn7003487

Albrecht MG, Creighton JA (1977) Anomalously intense Raman spectra of pyridine at a silver electrode. J Am Chem Soc 99:5215–5217. https://doi.org/10.1021/ja00457a071

Awada C, Barbillon G, Charra F, Douillard L, Greffet J-J (2012) Experimental study of hot spots in gold/glass nanocomposite films by photoemission electron microscopy. Phys Rev B 85:045438. https://doi.org/10.1103/PhysRevB.85.045438

Azziz A, Safar W, Xiang Y, Edely M, Lamy de la Chapelle M (2022) Sensing performances of commercial SERS substrates. J Mol Struct 1248:131519. https://doi.org/10.1016/j.molstruc.2021.131519

Barbillon G, Ivanov A, Sarychev AK (2021) SERS Amplification in Au/Si Asymmetric Dimer Array Coupled to Efficient Adsorption of Thiophenol Molecules. Nanomater 11:1521. https://doi.org/10.3390/nano11061521

Bodelón G, Pastoriza-Santos I (2020) Recent Progress in Surface-Enhanced Raman Scattering for the Detection of Chemical Contaminants in Water. Front Chem 8:1-8. https://doi.org/10.3389/fchem.2020.00478

Byram C, Moram SSB, Shaik AK, Soma VR (2017) Versatile gold based SERS substrates fabricated by ultrafast laser ablation for sensing picric acid and ammonium nitrate. Chem Phys Lett 685:103–107. https://doi.org/10.1016/j.cplett.2017.07.043

Cañamares MV, Chenal C, Birke RL, Lombardi JR (2008) DFT, SERS, and Single-Molecule SERS of Crystal Violet. J Phys Chem C 112:20295–20300. https://doi.org/10.1021/jp807807j

Carron KT, Hurley LG (1991) Axial and azimuthal angle determination with surface-enhanced Raman spectroscopy: thiophenol on copper, silver, and gold metal surfaces. J Phys Chem 95:9979–9984. https://doi.org/10.1021/j100177a068

Chen Q, Hassan MM, Xu J, Zareef M, Li H, Xu Y, Wang P, Agyekum AA, Kutsanedzie FYH, Viswadevarayalu A (2019) Fast sensing of imidacloprid residue in tea using surface-enhanced Raman scattering by comparative multivariate calibration. Spectrochim Acta - A: Mol Biomol Spectrosc 211:86–93. https://doi.org/10.1016/j.saa.2018.11.041

Chen J, Guo L, Qiu B, Lin Z, Wand T (2018) Application of ordered nanoparticle self-assemblies in surface-enhanced spectroscopy. Mater Chem Front 2:835-860. https://doi.org/10.1039/C7QM00557A

Dasary SSR, Singh AK, Senapati D, Yu H, Ray PC (2009) Gold Nanoparticle Based Label-Free SERS Probe for Ultrasensitive and Selective Detection of Trinitrotoluene. J Am Chem Soc 131:13806–13812. https://doi.org/10.1021/ja905134d

Ding S-Y, You E-M, Tian Z-Q, Moskovits M (2017) Electromagnetic theories of surface-enhanced Raman spectroscopy. Chem Soc Rev 46:4042–4076

Douillard L, Charra F, Fiorini C, Adam PM, Bachelot R, Kostcheev S, Lerondel G, Lamy de la Chapelle M, Royer P (2007) Optical properties of metal nanoparticles as probed by photoemission electron microscopy. J Appl Phys 101:083518. https://doi.org/10.1063/1.2719282

El Mendili Y, Bardeau JF, Randrianantoandro N, Gourbil A, Grenèche JM, Mercier AM, Grasset F (2011) New evidences of in situ laser irradiation effects on γ -Fe_2O_3 nanoparticles: a Raman spectroscopic study. J Raman Spectrosc 42: 239−242. https://doi.org/10.1002/jrs.2762

El Mendili Y, Bardeau JF, Randrianantoandro N, Grasset F, Grenèche JM (2012) Insights into the Mechanism Related to the Phase Transition from γ-Fe_2O_3 to α-Fe_2O_3 Nanoparticles Induced by Thermal Treatment and Laser Irradiation. J Phys Chem C 116: 23785−23792. https://doi.org/10.1021/jp308418x

Fedotova YV, Kukushkin VI, Solovyev VV, Kukushkin IV (2019) Spoof plasmons enable giant Raman scattering enhancement in Near-Infrared region. Opt Express 27:32578. https://doi.org/10.1364/OE.27.032578

Fleischmann M, Hendra PJ, McQuillan AJ (1974) Raman spectra of pyridine adsorbed at a silver electrode. Chem Phys Lett 26:163–166. https://doi.org/10.1016/0009-2614(74)85388-1

Gillibert R, Huang JQ, Zhang Y, et al (2018) Explosive detection by Surface Enhanced Raman Scattering. TrAC Trends Anal Chem 105:166–172. https://doi.org/10.1016/j.trac.2018.03.018

Grésillon S, Aigouy L, Boccara AC, Rivoal JC, Quelin X, Desmarest C, Gadenne P, Shubin VA, Sarychev AK, Shalaev VM (1999) Experimental Observation of Localized Optical Excitations in Random Metal-Dielectric Films. Phys Rev Lett 82:4520–4523. https://doi.org/10.1103/PhysRevLett.82.4520.

Halvorson RA, Vikesland PJ (2010) Surface-Enhanced Raman Spectroscopy (SERS) for Environmental Analyses. Environ Sci Technol 44:7749–7755. https://doi.org/10.1021/es101228z

He S, Kang MWC, Khan FJ, Tan EKM, Reyes MA, Kah JCY (2015) Optimizing gold nanostars as a colloid-based surface-enhanced Raman scattering (SERS) substrate. J Opt 17:114013. https://doi.org/10.1088/2040-8978/17/11/114013

Hou R, Pang S, He L (2015) In situ SERS detection of multi-class insecticides on plant surfaces. Anal Methods 7:6325–6330. https://doi.org/10.1039/C5AY01058F

Jeanmaire DL, Van Duyne RP (1977) Surface raman spectroelectrochemistry: Part I. Heterocyclic, aromatic, and aliphatic amines adsorbed on the anodized silver electrode. J Electroanal Chem Interfacial Electrochem 84:1–20. https://doi.org/10.1016/S0022-0728(77)80224-6

Kim J, Jang Y, Kim N-J, Kim H, Yi G-C, Shin Y, Kim MH, Yoon S (2019) Study of Chemical Enhancement Mechanism in Non-plasmonic Surface Enhanced Raman Spectroscopy (SERS). Front Chem 7:582. doi: 10.3389/fchem.2019.00582

Kumar G, Soni RK (2022) Trace-Level Detection of Explosive Molecules with Triangular Silver Nanoplates-Based SERS Substrates. Plasmonics 17:559–573. https://doi.org/10.1007/s11468-021-01544-0

Li S, Wu D, Xu X, Gu R (2007) Theoretical and experimental studies on the adsorption behavior of thiophenol on gold nanoparticles. J Raman Spectrosc 38:1436–1443. https://doi.org/10.1002/jrs.1791

Lin Z, He L (2019) Recent advance in SERS techniques for food safety and quality analysis: a brief review. Curr Opin Food Sci 28:82–87. https://doi.org/10.1016/j.cofs.2019.10.001

Liszewska M, Bartosewicz B, Budner B, Nasiłowska B, Szala M, Weyher JL, Dzięcielewski I, Mierczyk Z, Jankiewicz B (2019) Evaluation of selected SERS substrates for trace detection of explosive materials using portable Raman systems. Vib Spectrosc 100:79–85

Liu Y, Zhang Y, Tardivel M, Lequeux M, Chen X, Liu W, Huang J, Tian H, Liu Q, Huang G, Gilibert R, de la Chapelle ML, Fu W (2020) Evaluation of the Reliability of Six Commercial SERS Substrates. Plasmonics 15:743–752. https://doi.org/10.1007/s11468-019-01084-8

Magno G, Bélier B, Barbillon G (2017) Gold thickness impact on the enhancement of SERS detection in low-cost Au/Si nanosensors. J Mater Sci 52:13650–13656. https://doi.org/10.1007/s10853-017-1445-3

Mandal P, Tewari BS (2022) Progress in surface enhanced Raman scattering molecular sensing: A review. Surf Interfaces 28:101655. https://doi.org/10.1016/j.surfin.2021.101655

Mani S, Bharagava RN (2016) Exposure to Crystal Violet, Its Toxic, Genotoxic and Carcinogenic Effects on Environment and Its Degradation and Detoxification for Environmental Safety. In: de Voogt WP (ed) Reviews of Environmental Contamination and Toxicology Volume 237. Springer International Publishing, Cham, pp 71–104

Moram SSB, Shaik AK, Byram C, Hamad S, Soma VR (2020) Instantaneous trace detection of nitro-explosives and mixtures with nanotextured silicon decorated with Ag–Au alloy nanoparticles using the SERS technique. Anal Chim Acta 1101:157–168. https://doi.org/10.1016/j.aca.2019.12.026

Murugan E, Santhoshkumar S, Govindaraju S, Palanichamy M (2021) Silver nanoparticles decorated g-C3N4: An efficient SERS substrate for monitoring catalytic reduction and selective Hg2+ions detection. Spectrochim Acta - A: Mol Biomol Spectrosc 246:119036. https://doi.org/10.1016/j.saa.2020.119036

Noh J, Ito E, Hara M (2010) Self-assembled monolayers of benzenethiol and benzenemethanethiol on Au(111): Influence of an alkyl spacer on the structure and thermal desorption behavior. J Colloid Interface Sci 342:513–517. https://doi.org/10.1016/j.jcis.2009.10.076

Pérez-Jiménez AI, Lyu D, Lu Z, Liu G, Ren B (2020) Surface-enhanced Raman spectroscopy: benefits, trade-offs and future developments. Chem Sci 11:4563–4577. https://doi.org/10.1039/D0SC00809E

Rubira RJG, Camacho SA, Aoki PHB, et al (2014) Detection of trace levels of atrazine using surface-enhanced Raman scattering and information visualization. Colloid Polym Sci 292:2811–2820. https://doi.org/10.1007/s00396-014-3332-7

Scherrer D, Vogel D, Drechsler U, Olziersky A, Sparr C, Mayor M, Lörtscher E (2021) Scherrer D, Vogel D, Drechsler U, et al (2021) Monitoring Solid-Phase Reactions in Self-Assembled Monolayers by Surface-Enhanced Raman Spectroscopy. Angewandte Chemie International Edition 60:17981–17988. https://doi.org/10.1002/anie.202102319

Sivashanmugan K, Liao J-D, You J-W, Wu C-L (2013) Focused-ion-beam-fabricated Au/Ag multilayered nanorod array as SERS-active substrate for virus strain detection. Sens Actuators B: Chem 181:361–367. https://doi.org/10.1016/j.snb.2013.01.035

Sreekanth KV, Alapan Y, ElKabbash M, Ilker E, Hinczewski M, Gurkan UA, De Luca A, Strangi G (2016) Extreme sensitivity biosensing platform based on hyperbolic metamaterials. Nature Mater 15:621–627. https://doi.org/10.1038/nmat4609

Sun H, Liu H, Wu Y (2017) A green, reusable SERS film with high sensitivity for in-situ detection of thiram in apple juice. Appl Surf Sci 416:704–709. https://doi.org/10.1016/j.apsusc.2017.04.159

Taugeron P, Rahmani M, Delorme N, Douillard L, Bardeau J-F. How hot spot density and photo-emitted electron energy distribution reveal the performance of metal SERS substrates: A quantitative PEEM and Raman study. Submitted

Taugeron P, Rahmani M, Delorme N, Faure M, Douillard L, Bardeau J-F (2023) Quantitative PEEM and Raman Study of Nanorough Au SERS-Active Substrates for Molecular Sensing Applications. ACS Appl Nano Mater 6:11135–11143. https://doi.org/10.1021/acsanm.3c01050

Uchinokura K, Sekine T, Matsuura E (1972) Raman scattering by silicon. Solid State Comm 11:47–49. https://doi.org/10.1016/0038-1098(72)91127-1

Volný M, Sengupta A, Wilson CB, Swanson BD, Davis E.J, Tureček F (2007) Surface-Enhanced Raman Spectroscopy of Soft-Landed Polyatomic Ions and Molecules. Anal Chem 79:4543–4551. https://doi.org/10.1021/ac070278a

Wang S, Sun B, Feng J, An F, Li N, Wang H, Tian M (2020) Development of affinity between target and substrates in surface enhanced Raman spectroscopy for environmental pollutant. Anal Methods 12: 5657-5670. doi.org/10.1039/D0AY01760D

Wu T, Lin Y-W (2018) Surface-enhanced Raman scattering active gold nanoparticle/nanohole arrays fabricated through electron beam lithography. Appl Surf Sci 435:1143–1149. https://doi.org/10.1016/j.apsusc.2017.11.213

Ye Z, Li C, Chen Q, Xu Y, and Bell SEJ (2021) Self-assembly of colloidal nanoparticles into 2D arrays at water–oil interfaces: rational construction of stable SERS substrates with accessible enhancing surfaces and tailored plasmonic response. Nanoscale 13:5937-5953. DOI: 10.1039/D0NR08803J

Yi Z, Yi Y, Luo J, Li X, Xu X, Jiang X, Yi Y, Tang Y (2014) Arrays of ZnO nanorods decorated with Au nanoparticles as surface-enhanced Raman scattering substrates for rapid detection of trace melamine. Phys B: Condens Matter 451:58–62. https://doi.org/10.1016/j.physb.2014.06.026

Zhurikhina VV, Brunkov PN, Melehin VG, Kaplas T, Svirko Y, Rutckaia VV, Lipovskii AA (2012) Self-assembled silver nanoislands formed on glass surface via out-diffusion for multiple usages in SERS applications. Nanoscale Res Lett 7:676. https://doi.org/10.1186/1556-276X-7-676

(2000) Directive 2000/60/EC of the European Parliament and of the Council of 23 October 2000 establishing a framework for Community action in the field of water policy